JOURNAL OF GEOPHYSICAL RESEARCH, VOL. 100, NO. A2, PAGES 1883–1898, FEBRUARY 1, 1995

Dawn-dusk asymmetries in the low-latitude boundary layer arising from the Kelvin-Helmholtz instability: A particle simulation

M. Wilber and R. M. Winglee

Geophysics Program, University of Washington, Seattle

Abstract. Along the low-latitude boundary layer (LLBL), the Kelvin-Helmholtz (K-H) instability can provide a means for injection of solar wind plasma across closed field lines of the magnetosphere. A fully electromagnetic, two-dimensional (three-velocity) particle code is used to investigate dawn-dusk asymmetries that can arise from velocity differences due to gradient drifts and electric field gradients, and ion acceleration across the narrow field transition layers in the dawn and dusk flanks. The model includes the dawn and dusk sides of the LLBL simultaneously in a slab geometry, incorporating seperate populations of ions and electrons for the magnetosphere and the magnetosheath plasmas. We report several effects: (1) asymmetries in the observed morphology of the turbulent structures, with familiar fluidlike vortex formation on the duskside, but tongues of magnetosheath plasma penetrating into the magnetosphere on the dawnside; (2) the formation of discrete current layers, characterized by strong currents and sharp gradients in the magnetic field, and discrete charge layers, having net charges and constant, weaker currents; (3) increasing asymmetry in dawn/dusk behavior with a decrease of initial boundary layer width; and (4) enhancement of the dawn-to-dusk electric field as magnetosheath particles and momenta are transported across the magnetopause.

1. Introduction

At the start of the 1960s, *Axford and Hines* [1961] proposed a model of the magnetosphere, characterized by its convection patterns, which attempted to provide a unified explanation of the structure and location of many observed geophysical phenomena. These phenomena included aurorae, bay disturbances, ionospheric electron distributions, and the production of trapped particles in the outer Van Allen belt. Essential to this model was a driving mechanism which provided for transport of particles and momentum from the solar wind across the magnetopause. Earlier, *Dungey* [1955] had suggested that the magnetopause low-latitude boundary layer (LLBL) might be unstable to the Kelvin-Helmholtz (K-H) instability, and this was adopted as a candidate for the viscous interaction needed. Solar wind plasma can also enter the magnetosphere by reconnection, as proposed by *Dungey* [1961] and *Petscheck* [1964], but viscous interactions such as the K-H instability are probably most important for solar wind injection along the dawn and dusk flanks. Results of research to date have provided a strong observational and theoretical case for the existence of a magnetopause K-H instability. Observational evidence includes detection of polarized magnetic field pulsations at high-latitudes [*Atkinson and Watanabe,* 1966], and in situ [*Dungey and Southwood,* 1970], and motions of the magnetosphere boundary [e.g., *Williams,* 1980; *Couzens et al.,* 1985] in association with ultralow frequency (ULF) waves [*Allan and Poulter,* 1984].

Paper number 94JA02488.
0148-0227/95/94JA-02488$05.00

1.1. Linear Studies

Initial theoretical treatments of the K-H instability in magnetic fluids considered planar geometries and discontinuous jumps in the flow velocity [*Dungey,* 1955; *Chandrasekhar,* 1961; *Sen,* 1964; *Fejer,* 1964; *Southwood,* 1968; *Pu and Kivelson,* 1983]. Most of these authors found that the K-H instability would be stabilized for a velocity jump greater than a few times the sonic Mach number M_s. However, the physical relevance of this result was questioned. *Southwood* [1968] found that for large enough angles of propagation relative to the flow direction there would always be unstable modes regardless of the stability of the modes parallel to the flow.

Further questions about the stability of the magnetopause and the growth of the K-H instability were raised when the assumption of a discontinuous velocity jump was removed [*Blumen et al.,* 1975; *Drazin and Davey,* 1977]. These authors found no stabilizing upper bound for the velocity shear for ordinary, nonmagnetic, compressible fluids. *Papamoschou and Roshko*

[1988] verified this claim experimentally and explained the result by arguing that in a frame convecting with the velocity of the dominant mode, there is a region where the flow is subsonic, so the system should remain unstable. However, *Miura and Pritchett* [1982] analyzed compressible magnetic fluids having a velocity shear layer of finite thickness, and found that for a given flow speed the growth rates for the instability are maximized for $ka \sim 0.5 - 1.0$ (k is the wavenumber), and that a stabilizing upper bound for the velocity is twice the magnetosonic speed. These finite shear layer results point out the need to treat boundary thickness as a relevant parameter in K-H instability studies.

Linear, fluid studies indicate that the LLBL should be stable to the K-H instability near the subsolar stagnation point where there is little free energy in magnetosheath flows. (In actual circumstances, however, solar wind pressure variations can lead to enhanced plasma flows at the subsolar point, possibly leading to activation of the K-H instability there also.) In the tail, growth rates are expected to be small, because the magnetosheath flows become supersonic [*Miura,* 1992], and because the LLBL increases in thickness [*Haerendel et al.,* 1978; *Mitchell et al.,* 1987]. The analysis of *Miura and Pritchett* [1982] shows that the growth rates of the fastest growing modes vary with $\Delta v/a$, where Δv is the total velocity shear, and a is the thickness of the shear layer. In physical terms, increasing the thickness of the boundary layer inhibits the instability by increasing the wave crossing time.

The MHD results above have been supplemented by linearized, kinetic treatments [e.g., *Ganguli et al.,* 1988a; *Cai et al.,* 1990; *Fujimoto and Teresawa,* 1991; *Wang et al.,* 1992]. *Wang et al.* [1992] found that the growth rates and instability wavelength range could increase or decrease, depending upon the ratios of the velocity shear Δv, the Alfvén speed V_A, and the sound speed C_s, but that the instability threshold remained $V_A < \Delta v/2 < C_s$. *Ganguli et al.* [1988a] used a Vlasov approach, and *Opp and Hassam* [1991] used a modified MHD analysis to find a shear-driven electrostatic ion cyclotron-like instability that can dominate the K-H instability for short wavelengths. (Growth is maximized for wavelengths $\lambda \ll \pi a$ compared to maximum growth for the K-H instability when $\lambda \gtrsim \pi a$.) These short wavelength modes could be expected to coalesce into larger perturbations which could be seeds for K-H waves later on.

While the K-H instability requires a nonzero second derivative of the flow speed ($\partial^2 v_x/\partial^2 y \neq 0$), the inhomogeneous energy density driven instability found by *Ganguli et al.* [1988a] is sustained by differences in the energy density introduced by the local Doppler shift. It is further distinguished by the fact that it is enhanced by density gradients and when there is a finite parallel component of the wave vector ($\mathbf{k} \cdot \mathbf{B} \neq 0$). *Ganguli et al.* [1988c] and *Nishikawa et al.* [1988, 1990] have further demonstrated that Doppler shifts resulting from shear flow can lower the threshold for field-aligned electron drifts v_d that drive the current-driven ion cyclotron (CDIC) instability [*Drummond and Rosenbluth,* 1962], and can increase its wavelength. The presence of sufficiently strong field-aligned potentials will excite parallel CDIC modes which will compete with the K-H instability for available free energy.

Ganguli et al. [1988b], *Romero et al.* [1992] and *Romero and Ganguli* [1994] discuss electron-ion-hybrid and lower hybrid drift instabilities, which arise on short timescales $\omega_{LH}t \sim 10$ (ω_{LH} is the lower hybrid frequency). When an electric field is localized to a region L_E bounded by the electron and ion Larmor radii ($\rho_e < L_E < \rho_i$), and the shear parameter defined by $(\partial v_x/\partial y)_{max}/\omega_{LH}$ exceeds unity, the electron-ion-hybrid mode is excited. (For a species α the Larmor radius is $\rho_\alpha = q_\alpha B/m_\alpha c$, where q_α is the particle charge, m_α is its mass, and c is the speed of light.) This exhibits K-H-like signatures, having long wavelengths and flow circulation.

1.2. Fluid MHD Simulations

Computer simulations are critical for understanding the nonlinear behavior of the K-H instability, and during the past decade numerous researchers [e.g., *Miura,* 1982, 1984, 1987, 1990, 1992; *Wu,* 1986; *Belmont and Chanteur,* 1989; *Wei et al.,* 1990; *Wei and Lee,* 1993] have investigated the instability using fluid MHD techniques. In the series of papers cited, Miura presented a number of results linking observed boundary layer properties to the K-H instability. His models showed that the nonlinear evolution of K-H vortices can result in stresses and energy fluxes across the magnetopause that are large enough to account for the tailward LLBL flows observed in the deep geomagnetic tail. He computed values for an anomolous viscosity, which is an analog of the hydrodynamic eddy viscosity, that includes Maxwell stresses as well as Reynolds stresses. This anomolous viscosity indicates the "drag" on plasma flows caused by convecting vortex structures. Along the flanks of the LLBL this could readily exceed other sources of viscosity. Therefore, along the flanks the K-H instability may best satisfy the viscous boundary conditions required by the Axford and Hines model. Consistent with linear theory, Miura also found that the anomolous viscosity and transport were reduced as the magnetosheath magnetic field was set parallel to $\mathbf{v}$ and its magnitude increased. These models also verified that for flow speeds faster than the Alfvén speed, the magnetopause could be susceptible to the K-H instability even when $\mathbf{v}$ exceeded the sound speed in the magnetosheath.

It is important to note that in Miura's studies, the simulation boxes were no larger than the fastest growing mode (FGM) predicted by linear theory, and only slab geometries were considered. *Wu* [1986] addressed the system size problem with a simulation box 11 times the size of the FGM, and showed a growth rate identical to those of small, periodic systems. However, the wavelength of the disturbance expanded to about twice that of the FGM, and the amplitude grew unbounded, revealing that the saturation in earlier simulations had been artificially constrained by the periodic condition.

Wu's [1986] simulation was initialized with flat magnetic field and density profiles, which are not representative of common magnetopause conditions, and *Belmont and Chanteur* [1989] argued that his simulation was not run long enough to reveal a coalescence of FGM-sized modes to larger wavelength disturbances. Their own model, which was run for a greater duration, and which had some variation in magnetic and kinetic pressure across the boundary layer, demonstrated mode coalescence. As noted by *Miura* [1982] and others, it is generally true that a flat magnetic field scenario is more unstable than one where B varies, so magnetic field gradients need to be included in work intended to model the Earth's magnetosphere.

Wei et al. [1990] and *Wei and Lee* [1993] presented simulation results for a driven system with open boundaries downstream, rather than periodic boundaries. With $+x$ pointing tailward and $+y$ pointing into the magnetosphere, the main plasma flow was maintained at a fixed value v_x along the $y = 0$ edge of their box. In addition, a transverse "injection" flow $+v_y$ was maintained along that boundary. This either was constant along the entire boundary, or was nonzero only in a small region toward the sunward edge of the box. They found a thickening of the mixing layer toward the magnetotail, corresponding to the coalescence of smaller modes into larger modes downstream. This is consistent with observations by *Haerendel et al.* [1978] and *Mitchell et al.* [1987]. When the injection region was restricted to a small, sunward portion of the simulation box, the tailward thickening of the mixing layer remained bounded. The thickness grew indefinitely if the injection region was extended along the whole $y = 0$ edge of the simulation box. In order to minimize the viscosity built into their model, *Wei et al.* [1990] employed a high-order numerical differencing scheme. Even with this, they needed to run the code with a Reynolds number $R = (R_E \Delta v/\nu) < 2000$ in order to keep it stable. (R_E is one Earth radius, and ν is the viscosity.) Thus, in their work as well as that of the previously discussed authors, viscosity was instrumental in the development of the K-H instability.

1.3. Particle and Hybrid-Particle Simulations

Because the thickness of the LLBL can be of the order of a few ion gyroradii ρ_i, particularly on the dayside, intrinsic particle effects can be important. Since the ion Larmor radius is much larger than the electron gyroradius, ions penetrate further across magnetic field lines, producing space-charge effects. Gradient drifts within the boundary layers on the dawnside and duskside of the magnetosphere are oppositely directed with respect to the solar wind flow, resulting in a flow parallel temperature for ions T_{ix} which is greater on the duskside. We will show that this leads to an asymmetry in the onset of the K-H instability that is not included in current MHD models. In addition, MHD is a single-fluid treatment, so the relative mixing and heating of magnetosheath and magnetosphere populations cannot be identified. Finally, fluid codes rely on the addition of an artificially imposed viscosity term to produce the K-H instability, which in turn generates the anomolous viscosity sought.

A number of authors [*Pritchett and Coroniti,* 1984; *Pritchett,* 1987; *Nishikawa et al.,* 1988, 1990; *Teresawa et al.,* 1992; *Thomas and Winske* 1991, 1993] have used particle simulations and hybrid simulations (to be discussed) to overcome some of the limitations mentioned above. Using electrostatic codes, *Pritchett and Coroniti* [1984] examined the finite Larmor radius influences on the K-H instability. They found that for values of the ratio $\rho_i/a < 0.5$ the fluid treatments are accurate but that larger values result in a strong suppression of the instability. *Pritchett and Coroniti* [1984] also observed the coalescence of short wavelength modes into larger modes, which led them to suggest that boundary curvature may ultimately determine the size of actual K-H vortices. In these simulations the initial density, temperature, and magnetic field profiles were flat, and the use of purely electrostatic simulations did not allow for evolution of the magnetic fields.

Nishikawa et al. [1988], *Teresawa et al.* [1992], and *Thomas and Winske* [1991, 1993] have employed hybrid particle codes for modeling the K-H instability. Hybrid codes, which treat the electrons as a fluid and the ions as individual particles, have the advantage that they can incorporate larger scale lengths and longer time scales than particle simulations. *Nishikawa et al.* [1988, 1990] sought to show the importance of the ion-cyclotron modes [*Ganguli et al.,* 1985, 1988], which can compete with and dominate the K-H instability for high spatial frequencies. This is especially true when the flow velocity has a small component parallel to **B**, for which case the K-H modes have significantly reduced growth rates. *Ganguli et al.* [1988a] presented an analytic kinetic treatment of plasmas with shear flows. They obtained a distribution function with $\Delta v/a\Omega_i$ corrections to a Maxwellian, that incorporates the effects of electric field gradients on particle $\mathbf{E} \times \mathbf{B}$ drifts. (Ω_i is the usual ion gyrofrequency.) When *Nishikawa et al.* [1988] employed this in their simulation loading scheme they obtained growth rates for the K-H instability which were higher than those for the Maxwellian loading used by *Pritchett and Coroniti* [1984].

Thomas and Winske [1991, 1993] studied the K-H instability in the low latitude boundary layers of the Earth and Venus, incorporating distinct, interacting ion populations for the magnetosheath and magnetosphere. Both ion populations had the same temperature, but initial field and density profiles varied across the simulation box. Their models showed detachment of ion blobs with sizes of order ρ_i on both the magnetosphere and magnetosheath sides of the boundary layer, which were left behind as the K-H vortices wrapped up. More importantly, these simulations showed a filamentary structure in the instability, which contrasts considerably with the vortex structure typical of fluid studies. *Thomas and Winske* [1993] analyzed the mass transport across the midplane of the simulation box, and found it to be comparable to rates found by *Miura* [1984], and that it decreased as the difference between the magne-

tosphere and magnetosheath field strengths increased, corresponding to the reduction in vortex behavior seen.

In this paper we use particle simulations to show that the development of the K-H instability and the structure of the LLBL are strongly determined by intrinsic particle effects. These effects produce distinctive features, not previously identified, in the structure of the LLBL and in the velocity distributions of the ions. In section 2 we summarize our model. Features which distinguish it from previous work include (1) integration of both the dawnside and duskside of the LLBL into a simplified simulation box; (2) inclusion of distinct electron populations as well as ion populations for both the magnetosphere and the magnetosheath, (3) initial field and pressure gradients; and (4) a fully electromagnetic treatment of fields and particle motions.

In section 3 we present results from our model and provide a detailed study of a representative case with $\rho_i/a = 0.4$. (Here, and in what follows, ρ_i/a refers to an average of the Larmor radii for both ion populations divided by the width scale parameter.) This section provides an overview of the early evolution of the system, and of the morphology of the instabilities that develop (section 3.1). We show that with kinetic effects included in our model, the duskside is susceptible to earlier onset of the K-H instability than is the dawnside. These duskside perturbations evolve into vortices similar to those found in fluid MHD studies, but the dawnside perturbations, while also circulatory, exhibit a filamentary form similar to those shown by *Thomas and Winske* [1993], who used a hybrid-particle model. These morphological differences, which are here attributed to finite Larmor radius influences on the nonlinear evolution of the system, are reproduced even though the particle code was run with a reduced ion-electron mass ratio.

One of the advantages of the particle simulations is that they explicitly reveal, for the first time, structures that form in the boundary layers. On the dawnside, these structures resemble features found in ISEE magnetopause crossings by *Song et al.* [1990, 1993] (section 3.2). Structures seen in our simulations include a strong current layer, an exterior transition layer, and an interior transition layer. These transition layers are characterized by uniform, weak currents and the mixing of magnetosheath and magnetosphere populations, with the interior transition layer containing the net charges required for the gradients in the cross-tail electric field.

Particle velocity distributions are also important as they can be used to identify the relative roles of heating and mixing in the boundary layers (section 3.3). There is strong heating in v_y (perpendicular to **B** and **v**) in the dawnside LLBL, but minimal v_y heating on the duskside. In boundary layer distributions of v_x, both sides exhibit high-energy tails in the direction of the gradient drifts. Particle counts indicate some mixing of populations in the boundary layer.

In section 3.4 we compare results for narrower ($\rho_i/a = 0.8$) and wider ($\rho_i/a = 0.25$) boundary layers. These show a trend toward increasing dawn-dusk asymmetry as ρ_i/a increases, and an inhibition of the instability on the dawnside in the limit of a thin boundary. Last, in section 4 we summarize our results, and state our plans for future work.

2. The Model

For this study of the K-H instability we have used a two-dimensional (three-velocity), fully electromagnetic particle-in-cell code [*Winglee and Kellogg,* 1990], which allows for self-consistent evolution of electrostatic and electromagnetic fields. The short scale-length electrostatic quantities are solved on fine 256×512 grids, and longer-wavelength electromagnetic quantities are solved on grids with half this resolution. This dual gridding saves computer memory and time, without the loss of significant physics. The simulations are in the equatorial plane, with the initial magnetic field $\mathbf{B} = B(y)\mathbf{z}$ directed out of the simulation box ($\mathbf{k} \cdot \mathbf{B} = \mathbf{0}$). The flow velocity **v** is in the x direction, and field and density gradients are in the y direction. The system is periodic in both the x and y directions. For the values of a used here, there was no interaction of the regions across the top and bottom edges, and the periodic condition eliminated the large charge buildups that had developed when reflection boundaries were employed.

The geometry of the system modelled is shown in Figure 1. The top half of the system is used to represent the dawn LLBL, and the bottom half represents the dusk LLBL. The inclusion of both the dawn and dusk sides of the boundary layer in this simulation is valid provided there is little or no interaction between the two. This is true in the present case because the particles only slowly convect across the system. This simulation does not incorporate any effects due to the curvature of the LLBL, and the absence of components of the magnetic field in the simulation plane prevents excitation of the electrostatic ion cyclotron modes described by *Ganguli et al.* [1988a, c]. Assuming 2-keV ions and a 30-nT magnetic field in the magnetosheath, the system scales to 2500 km $\times$ 5000 km in physical units.

There are four distinct particle populations studied in this model: ions and electrons in the magnetosphere and in the magnetosheath. The ions and electrons making up the magnetosphere plasma are hot and rarified, while the particles of the magnetosheath plasma are cool and dense, and for either plasma the two component species are initialized to have the same temperature. The magnetosheath temperature is 2/5 the value for the magnetosphere, and the densities are larger by a factor of 16. The corresponding plasma beta's ($\beta = 8\pi p/B^2$, with p the thermal pressure) are 1.3 in the magnetosheath and 0.10 in the magnetosphere.

Particles are initialized with Maxwellian velocity distributions having a bulk flow v_x which varies linebreak as $\pm\tanh(y/a)$ across the dusk and dawn boundary layers, respectively. The initial magnetic field varies with a $\mp\tanh(y/a)$ profile, increasing by 45% in the magnetosphere. The width of the current sheet is initially the same as that of the bulk flow shear layer. Observations show the latter to be much thicker than the former, but we show later that the evolved system results in a substantial widening of the velocity

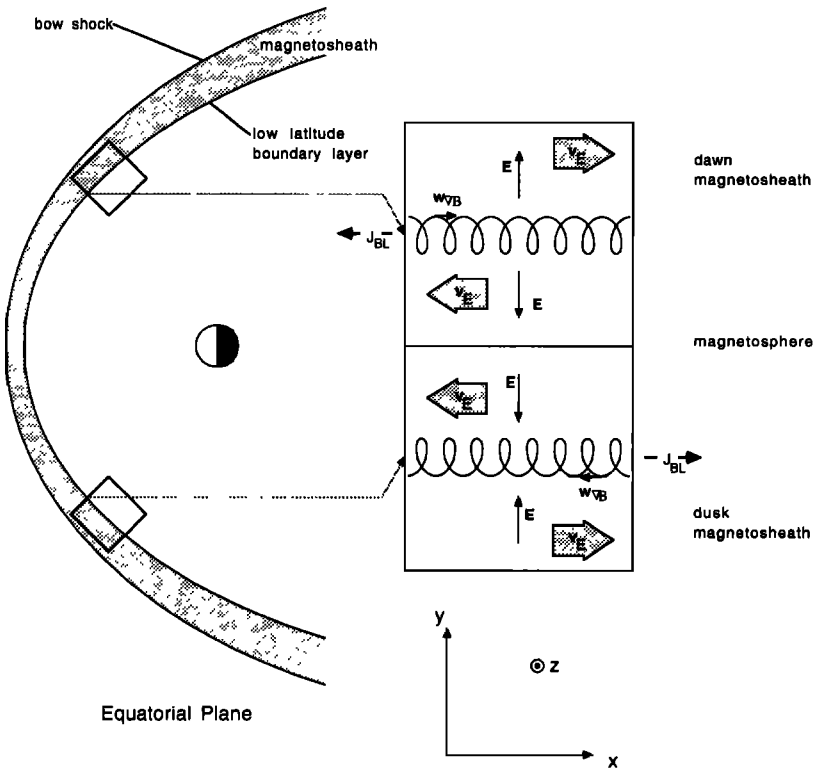

Figure 1. Simulation Geometry. Two squares representing the dawnside and the duskside of the low latitude boundary layer are joined to make the simulation box, with the interior corresponding to the magnetosphere and the top and bottom edges representing the magnetosheath. Note the directions of the dawn and dusk currents $\mathbf{J}_{\mathrm{BL}}$, and ion gradient drifts $\mathbf{w}_{\nabla B}$.

shear layer. The flow at the edges and the center correspond to sonic Mach numbers $M_s = v/C_s$ in the magnetosheath (magnetosphere) of 0.94 (0.41), and Alfvén Mach numbers $M_A = v/V_A$ of 1.08 (0.13), respectively.

In addition to the $\tanh(y/a)$ velocity profile, a small differential flow between electrons and ions is added so that Ampere's law, $\mathbf{J}_{BL} = \sum n_{cell} q_j \mathbf{v}_j = (c/4\pi)\nabla \times \mathbf{B}$, is satisfied. (Here q_j and $\mathbf{v}_j$ are charges and velocities of each particle found in a given grid location, and n_{cell} is a normalization factor used to maintain consistent statistics for all populations.) As indicated in Figure 1, the dawnside boundary layer represented in the top half of the simulation box has $\mathbf{J}_{\mathrm{BL}}$ pointing sunward, while the duskside boundary layer has it pointing tailward. The net current of the system therefore is zero.

Pressure balance was established with initial number densities set by

$$n(y) = \frac{n_{sh}(e^{-2y/a} + \zeta) + n_{sp}(e^{2y/a} + \zeta)}{(e^{-y/a} + e^{y/a})^2} \qquad (1)$$

where n_{sp} and n_{sh} are the limiting electron/ion densities for the magnetosphere and magnetosheath, respectively; and ζ has the form

$$\zeta = 2\frac{(1+\beta_{sp})(1+\beta_{sh}) - \sqrt{(1+\beta_{sp})(1+\beta_{sh})}}{\beta_{sh} + \beta_{sp} + 2\beta_{sh}\beta_{sp}} \qquad (2)$$

In order to sustain the local shear flow $\mathbf{v}$, a convective electric field was setup using a small excess charge distribution matching $1/(4\pi)\nabla \cdot \mathbf{E}$. (Opposite charge excesses in the two boundary layers ensured overall charge neutrality.) Profiles of the initial magnetic field, bulk plasma velocity, net charge density, and plasma particle number densities are shown in Figure 2. The particle densities and the magnetic field are normalized by the nominal magnetosheath values. The charge density is normalized by ρ_{q0}, the maximum initial charge density (i.e., $(1/4\pi)[\nabla \cdot \mathbf{E}]_{max}$).

Each simulation was run with a total of approximately 380,000 particles. To maintain consistent statistics, fractional masses and charges (keeping the ratio q/m fixed) were employed for the two magnetosphere populations. This allowed for an initially constant particle count throughout the system of ~ 3 particles per electrostatic cell ($\sim$ 12 particles per electromagnetic cell) while the mass density varied by a factor of up to 16 across the system. An artificially low ion to electron mass ratio of 16 was used in all of the runs presented here, which permitted inclusion of electrostatic scales, determined by the electron Debye length, in a system containing a large number (of order 100) of ion Larmor radii. In addition, the low mass ratio enabled the code to run at a feasible speed as this made the electron and ion gyroperiods more comparable. The small mass ratio does not seem to affect the results strongly, as the observed growth rates and structures are similar to those seen in MHD and hybrid simulations. (We can expect that where particle effects are important, a low mass ratio would only underestimate the resulting asymmetries.) Even with the low mass ratio of 16, our system

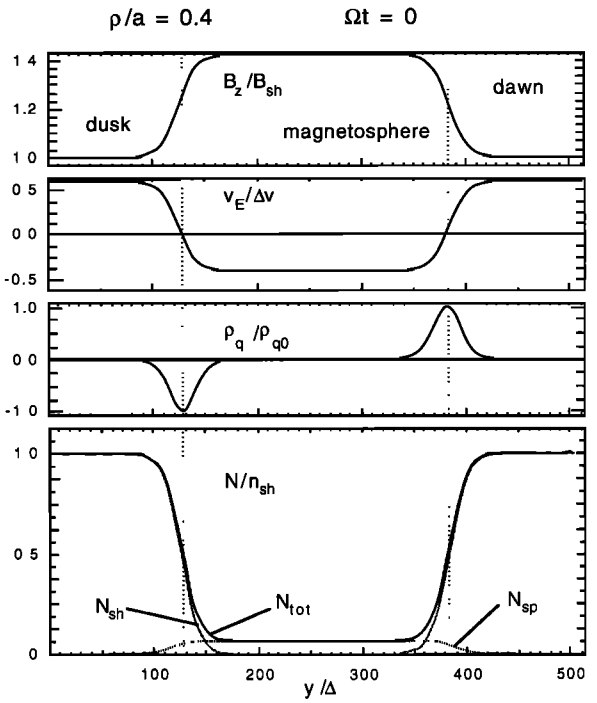

Figure 2. Initial simulation profiles for $\rho_i/a = 0.4$. Shown above are profiles, averaged over x, of initial magnetic field B_z, flow velocity v_x, total charge density ρ_q, and population densities n_{sh}, n_{sp} and n_{tot}. The normalization charge density ρ_{q0} is the maximum of $(1/4\pi)\nabla \cdot \mathbf{E}$ for the initial field configuration. The vertical lines show the location of the centers of the magnetic boundary and velocity shear layers.

size was of the order of the linear, fastest growing mode, although for the case of $\rho_i/a = 0.8$ the system was > 2 FGMs.

The use of Maxwellian distribution functions to approximate equilibrium for K-H instability simulations has been criticized previously [*Ganguli et al.*, 1988a; *Nishikawa et al.*, 1988]. However, an appropriate analytic model had not been found for the case of velocity shears in the presence of strong magnetic field, density and temperature gradients by the time of this study. Recently, *Romero et al.* [1992] and *Romero and Ganguli* [1994] have found more general, self-consistent loading schemes that include field and density (but not temperature) gradients. We show next that within several ion gyroperiods, before effects of the K-H instability are evident, the particle distributions adjust in a manner that can be consistent with these Vlasov schemes. [*Ganguli et al.*, 1988a]. While this state may not perfectly reflect true equilibrium conditions, and some free energy may be lost from the bulk flow to the adjusted particle distributions, the actual LLBL is subject to constant changes in external conditions, and may only rarely reach a true equilibrium.

3. Results

The Maxwellian loading of the particles is only an approximation of equilibrium conditions in the boundary layers, because the presence of gradients in the fields and densities can lead to the partial mixing of different plasma populations, and because particle-drift-related effects will otherwise distort the distributions. Figure 3a shows the equilibrium velocity distributions in the midboundary layer for magnetosheath and magnetosphere ion populations after this mixing has occurred. The timescale for this mixing $\Omega_i^{sp} t \lesssim 13$ is well before any growth of the K-H instability. Rectangles in the insets indicate the locations of sampling slices in the simulation box. The dawnside distributions have an increased spread in v_y, the direction perpendicular to the flow, while on the duskside the increased spread is in v_x.

The formation of these distributions can be understood by referring to the schematic in Figure 3b. Hot

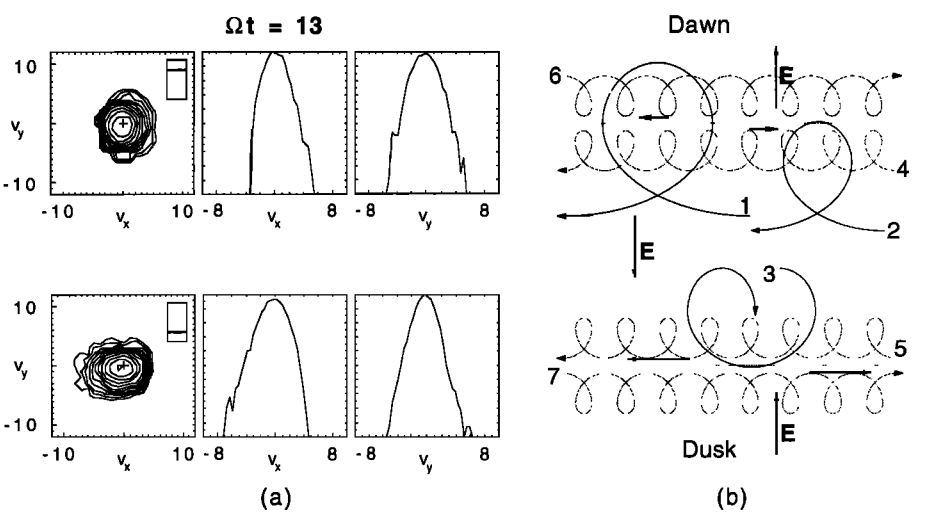

Figure 3. Early ion velocity distributions ($\rho_i/a = 0.4$, $\Omega_i^{sp} t = 13$). (a) Mid-LLBL ion distributions early in simulation (velocities are given in units of the magnetosheath ion thermal speed v_{ti}^{sh}); (b) representative orbits on dawnside and duskside. (See main text.)

magnetospheric particles, having gyroradii $> a$ are illustrated by trajectories 1–3 (solid lines). Trajectory 1 corresponds to a sunward directed magnetosphere ion whose gyromotions take it across part of the dawn boundary layer. The size of the orbit can be large since magnetospheric temperatures are high, particularly for particles in the high-energy tail of the distribution. As this particle crosses the center of the dawn boundary layer, it is pulled further away from the magnetosphere by the magnetosheath electric field. This orbit contributes to the $\pm v_y$ tails (perpendicular to **B** and **v**) in the dawnside distributions. Particles originating further from the boundary layer (represented by the second trajectory) would reach the midboundary layer at the top of their orbits, contributing to the $+v_x$ tail. Trajectory 3 originates the same distance from the dusk boundary layer as trajectory 1 does from the dawn boundary layer, and the particle has the same thermal speed as particle 1. This orbit does not extend as far into the magnetosheath as trajectory 1 does because the magnetosheath electric field opposes the entry of ions into that region. If particle 3 reaches the middle of the boundary, its motion there is primarily sunward, adding to the $-v_x$ tail in the dusk distribution. Gradient drifts $\mathbf{w}_{\nabla B}$ add to the asymmetries in v_x, since they are tailward on the dawnside and sunward on the duskside.

Cold particles having gyroradii $< a$ are represented by trajectories 4–7 (dotted curves). Trajectories 4 and 5, both centered to the interior of the LLBL, $\mathbf{E} \times \mathbf{B}$ drift sunward, while trajectories 6 and 7 drift tailward. On the dawnside, the orbits of particles 4 and 6 overlap in the center of the LLBL, indicated by the horizontal dotted line. When touching this line, each particle has a minimum speed because its orbital velocity there is directed opposite to its $\mathbf{E} \times \mathbf{B}$ drift velocity. The resulting spread in v_x is small. On the duskside, particles 5 and 7 overlap where their speeds are maximum, because their orbital velocities are aligned with their drift velocities. The spread in v_x on that side is therefore large.

We make a final observation about the equilibrium distributions: when the magnetosphere and magnetosheath populations are considered separately, the temperature dependence of gradient drifts leads to changes in the relative velocities between the two. On the dusk side the gradient drifts are in the $-x$ direction, and the hotter magnetosphere ions acquire a greater sunward speed change than do the magnetosheath ions. The result is an increase in the relative velocity. On the dawn side the drifts are tailward and the magnetosphere ions acquire a velocity change in the direction of the magnetosheath flow. This reduces the relative flow between the populations in that boundary layer. This effect can be seen in profiles of the separate magnetosheath and magnetosphere flows (not shown).

3.1. Morphology of the K-H Instability on the Dawnside and Duskside of the LLBL

The simulations presented here are parameterized by ρ_i/a, which relates the relevent scale for kinetic effects to the scale length of the initial magnetopause. For 2-keV magnetosheath ions in a 30-nT magnetic field, ρ_i/a ranging from 0.25 to 0.8 implies initial current layer thickness from about 160 km to about 490 km. While these widths are small compared to values typically observed, our simulations show the development

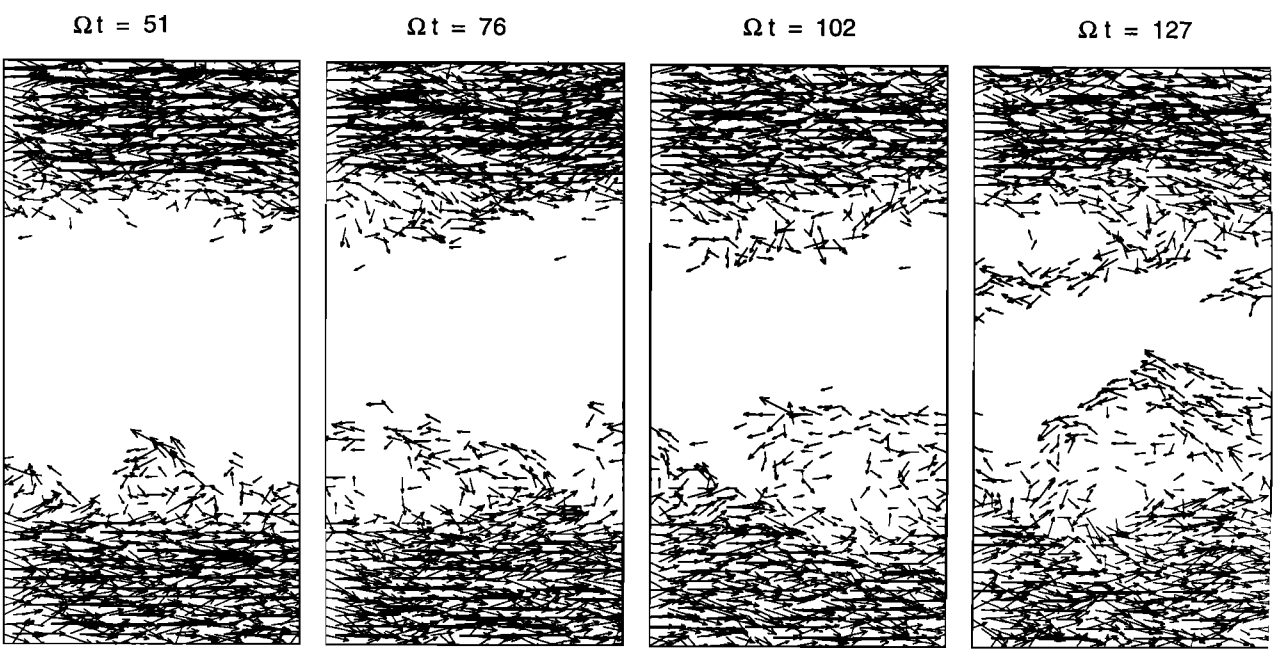

Figure 4. Magnetosheath electron momentum densities for $\rho_i/a = 0.4$. Arrows correspond to momentum densities averaged over 4 × 4 electromagnetic simulation grids. As the instability progresses, the dusk side shows vortex structure common to fluid models, while the dawn side develops a "tongue" which projects into the magnetosphere.

of the K-H instability leads to a broadening of the magnetopause to widths between 1000 and 1600 km.

Figure 4 shows the time-evolution of the magnetosphere electron momenta for the case $\rho_i/a = 0.4$. Prior to $\Omega_i^{*p}t = 51$ the duskside momenta show the emergence of small-amplitude modes, with wavelengths a quarter to a third the size of the simulation box. These disturbances grow larger in successive frames, and coalesce into a single system-wide mode by $\Omega_i^{*p}t = 127$. Nearly from the onset, the K-H instability on this side is characterized by vortex motions, and these persist as the modes coalesce until the final saturation structure breaks up. This behavior is consistent with that exhibited by fluid MHD models [e.g., *Miura*, 1987, 1992; *Belmont and Chanteur*, 1989].

On the dawnside there is no distinct wave growth until about $\Omega_i^{*p}t = 76$, which is after the start of the K-H instability on the dusk side. The dawnside also differs in that the disturbance emerges with a wavelength more than double that seen in the initial structures on the duskside. This dawn side perturbation remains close to the initial boundary layer position through $\Omega_i^{*p}t = 102$. Between $\Omega_i^{*p}t = 102$ and $\Omega_i^{*p}t = 127$ the disturbance extends away from the original LLBL, forming a "tongue" approximately 45 grid units across (roughly $5\rho_i$ for magnetospheric ions), which projects well into the magnetosphere. As this structure extends it loses its coherence, and breakup occurs in the last frame. This tongue feature is unique to the dawnside, and is similar to the filamentary structures seen in hybrid particle simulations by *Thomas and Winske* [1993]. This dawnside behavior, which is not seen in fluid studies, indicates that particle effects can be seen with our simulations that use a ion-electron mass ratio of 16.

Particle simulations are important because the asymmetric onset of the K-H instability is a consequence of kinetic effects. The initiation of the instability differs because there is a greater flow-parallel ion temperature T_{ix} on the duskside, as discussed earlier (see Figure 3). This implies a larger range of relative motions for ions sampled at a given y-value in the dusk current layer. The nonlinear development also differs, and this is likely due to particle effects as well, although the details are complex. In particular, there is evidence for a diffusive penetration of dusk-side particles into the magnetosphere as seen in the ion density contours of Figure 5. In contrast, dawn-side contours show coherence in the boundary layer, even after it has been substantially perturbed.

Superposed on top of the density contours of Figure 5 are electric field vectors. Early on ($\Omega_i^{*p}t = 51$), there is a reversal of **E** within the boundary layers on both the dawn and dusk sides of the LLBL. To a good approximation, the field orientations are normal to the density contours, reflecting $\mathbf{E} \times \mathbf{B}$ drifts transverse to the density gradients. Successive panels show that as the perturbations grow, these field vectors continue to realign themselves to maintain boundary normal orientations. At later times, the width of the dawn-to-dusk pointing electric field region in the center decreases, and there is a corresponding increase in the strength of the field there. These perturbed electric fields contribute to differences between the instabilities on the dawnside and duskside during the late stages.

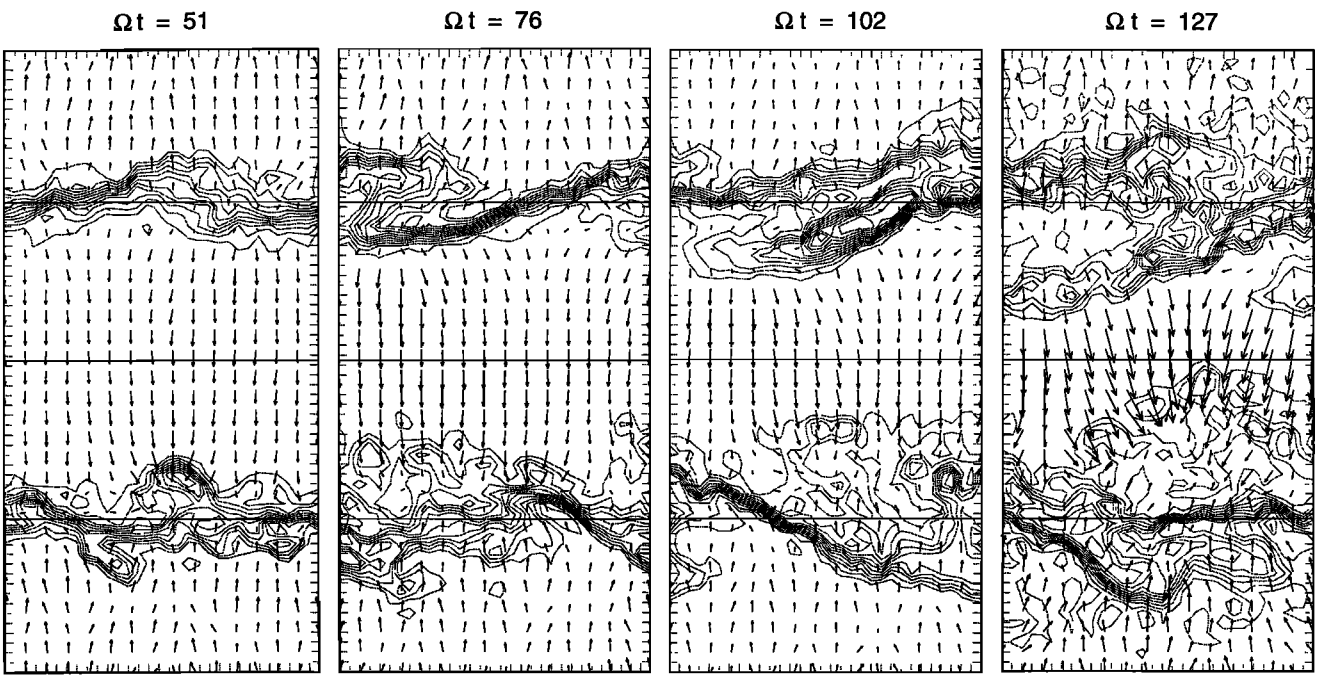

Figure 5. Electric field vectors superposed on magnetosheath electron density contours ($\rho_i/a = 0.4$). On the duskside the magnetopause develops a sawtooth form, while on the dawnside, the perturbation folds over and emerges as a "tongue"-shaped feature. Note that in the right panel the field vectors point into the duskside vortex, and away from the magnetospheric pocket exterior to the dawnside "tongue".

In the presence of strong field gradients occuring over length scales comparable to ρ_i, ions do not merely follow $\mathbf{E} \times \mathbf{B}$ and gradient drift motions. In addition, they undergo slow accelerations in the direction of the electric field. Around $\Omega_i^{sp}t = 102$ the dawnside perturbation begins to push into a region where $\mathbf{E}$ points dawn-to-dusk, rather than dusk-to-dawn. From this point, ions on the interior edge are drawn further into the magnetosphere, with an accelerated movement of the "tongue" feature towards the center. This duskward flow of magnetosheath ions in the dawnside perturbation is illustrated in Figure 6, which shows ion and electron momentum vectors for $\Omega_i^{sp}t = 127$. (The horizontal gaps in the ion flows are due to a plotting threshold, which eliminates points in regions of low speed or density. Electron plots do not show these gaps in the low-flow regions due to their greater thermal speeds.) The dashed horizontal line indicates the furthest extent of the ion flows into the magnetosphere. In these plots, it is clear that the ion flows on the dawnside have an interior edge that extends further into the magnetosphere than do the electron flows. This difference is due to the larger Larmor radii of the ions. Electrons, with their small gyroradii, do not experience significant accelerations parallel to $\mathbf{E}$.

As expected for regions of where the vorticity $\nabla \times \mathbf{v}$ is antiparallel to $\mathbf{B}$, the electric field vectors point away from the pocket of magnetospheric plasma that forms above the dawnside tongue by $\Omega_i^{sp}t = 127$, and similarly point into the vortex on the duskside. Such electric field patterns imply positive charge excesses in the plasma pocket on the dawnside, and negative net charges in the dusk vortex. These two charged areas are located in regions on the magnetosphere side of the magnetopause, corresponding to closed field lines that would map to the ionosphere, and have signs consistent with the region 1 field-aligned currents seen in the auroral oval. (See also the charge profiles of Figure 7a described next.) *Lui et al.* [1989] have suggested that the periodic bright spots ("pearls") seen in ultraviolet images obtained by the Viking satellite may correspond to modulations of vortex-driven field-aligned currents by the K-H instability.

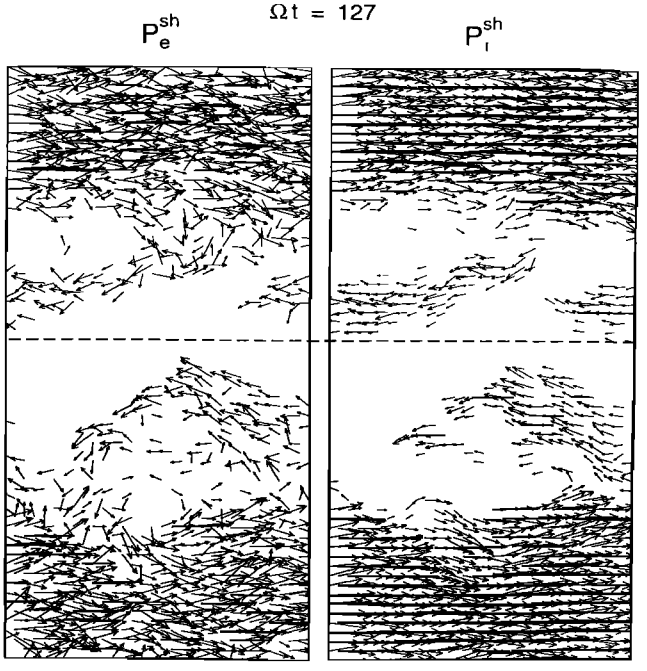

Figure 6. Comparison of ion and electron flows ($\rho_i/a = 0.4$; $\Omega_i^{sp}t = 127$). Electron momentum density vectors are plotted on the left, with ion momentum densities on the right. The dotted line shows the limit to which the ion flows have extended into the magnetosphere.

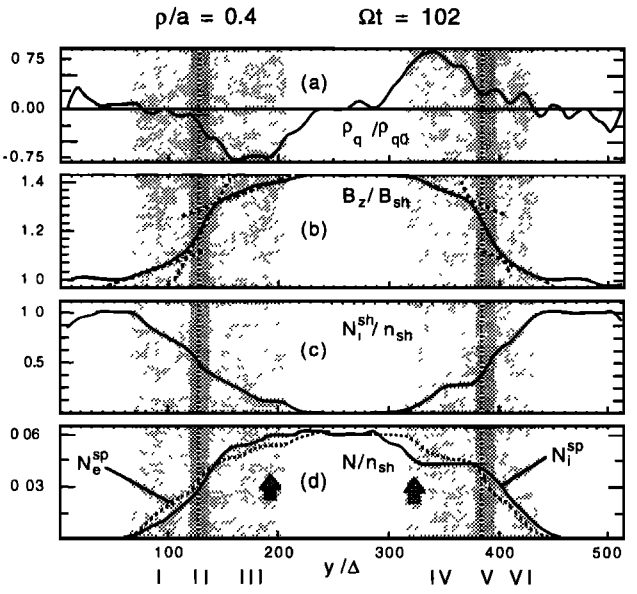

Figure 7. Profiles for $\rho_i/a = 0.4$, $\Omega_i^{sp}t = 102$. (a) ρ_q; (b) B_z; (c) magnetosheath ion density; (d) magnetosphere ion and electron densities. The shaded regions highlight magnetopause structures that are formed on the two sides of the magnetosphere. (See text for explanation.)

3.2. Structures of the Boundary Layer and Associated Asymmetries

With the development of the K-H instability, and the redistribution of the convective electric field, the original charge and current layers separate to produce distinct structures in the LLBL. Figure 7a shows a profile of the total charge density averaged over x at $\Omega_i^{sp}t = 102$. Centers of the initial LLBL are shown as dotted vertical lines. We can see that the charge layers in the dawnside and duskside of the boundary layer (shaded areas III and IV) have migrated in toward the magnetosphere. In addition, they have broadened considerably compared to their original widths (Figure 2), which is more consistent with observed velocity shear layer thicknesses that are $\gtrsim$ 600km. These charge layers are the sources for the electric field reversals seen in Figure 5. A profile of the magnetic field is shown in Figure 7b. On both the dawnside and the duskside, this has three regions where the slopes are relatively con-

stant (dotted tangent lines). The steepest gradients, indicating strong current layers, are near the original boundary layer and are denoted by dark shading (regions II and V).

Surrounding these current layers are transition regions (lightly shaded areas), where there also is a mixing of magnetosheath and magnetosphere particle populations, as shown in Figure 7c and Figure 7d. (Magnetosheath electron densities do not differ enough from ion densities to show up well on the scale of Figure 7c.) The interior transition regions (III and IV) are characterized by a magnetospheric density close to the nominal center density n_{sp}, and a magnetosheath population which is substantially reduced from its density outside the magnetopause n_{sh}. Across most of the interior transition region on the duskside the magnetosheath density falls uniformly from $\approx 0.4n_{sh}$, but on the dawnside the density remains constant at $\approx 0.3n_{sh}$ through half of this transition region. The exterior transition regions (I and VI) have magnetosheath components typical of the actual magnetosheath, with magnetosphere contributions substantially reduced from n_{sp}. Although the current layers have widths similar to their initialization values, when the transition regions are included, the resulting LLBL is more than 4 times wider than originally on both the dawnside and the duskside.

The net charges that are neccesary to support the gradients in the cross-tail electric fields (Figure 5) are located in the interior transition regions, with a net positive charge in the dawn-side region, and a net negative charge on the dusk side. However, the density profiles in Figure 7d indicate that for the magnetosphere plasma considered alone there is a net positive charge in region III and a net negative charge in region IV (large arrows). These arise as the magnetosphere ions migrate along the direction of **E**. Because these ions are hot, finite Larmor radius effects are greater than for their cold population counterparts. With abundant magnetosheath particles available to supply the overall charge needed (Figure 7a), the magnetosphere ions are free to drift along **E**. This is also seen in regions exterior to the charge layers, where **E** points dusk-to-dawn and the hot magnetosphere ions have shifted towards dawn.

The actual LLBL is known to exhibit structure similar to what is presented here. For example, dawnside features of the profiles in Figure 7 resemble the structures described by *Song et al.* [1990] and *Song et al.* [1993], in reference to the ISEE 1 encounter with the dayside LLBL on November 1, 1978. These authors identified three regions in the boundary layer. (Refer to Figure 1 of their 1990 paper.) Just inside the magnetosheath was a "sheath transition layer", characterized by a linear fall in density and a corresponding rise in the magetic field, which resembles the exterior transition layer described above. Inside this there was an abrupt drop in particle counts, and a jump in the strength of the magnetic field, much like our current layer. The field and density discontinuities observed demark the edge of an "outer boundary layer". In this outer boundary layer, the density and magnetic field strength remained constant, as is seen for half of our interior transition region on the dawnside. A second drop in the observed density, accompanied by a jump in temperature, signaled the start of an "inner boundary layer". The increase in temperature here represented a tripling of magnetosphere ions, which were now half of the total count. A final doubling of temperature as the magnetosheath ion component fell to zero indicated the start of the magnetosphere proper. In the profiles of Figure 7 there are increases in the temperature and in the relative magnetosheath proportion of the plasma, but the abrupt transitions to the inner boundary layer and the magnetosheath seen by *Song et al.* [1990] are not present. If the interior and exterior regions are included the final widths of the dusk and dawn boundary layers are $\sim$ 1400 and 1200 km, respectively.

The correspondence between our profiles in Figure 7 and the boundary structures inferred from ISEE 1 data by *Song et al.* [1990] is crude, and we should expect it to be. To make their determinations, those authors worked with data from the quietest subsolar boundary crossings in a 10-year sample. We, on the other hand, are modeling a highly disturbed boundary in regions where strong magnetosheath flows are likely to affect the structure of the LLBL. Our averages along a boundary that is strongly perturbed blurs transitions that are sharp along a single cut. The plateaus in the dawn side densities correlate closely to the coherent structure seen penetrating into the magnetosphere in Figure 5, and the intermediate values for these densities can be viewed as a consequence of the averaging in x across alternating magnetosheath and magnetosphere regions. The lack of definition in the dusk side profiles at $\Omega_i^{sp}t = 102$ reflects the enhanced circulation of plasma across the LLBL due to the strong vortex motion, and the diffusive mixing that is revealed by the density contours (Figure 5). *Wei et al.* [1990] modeled the K-H instability in the dawn LLBL, and reported plateau formation in a "mixing region". However, it appears as though here it is actually

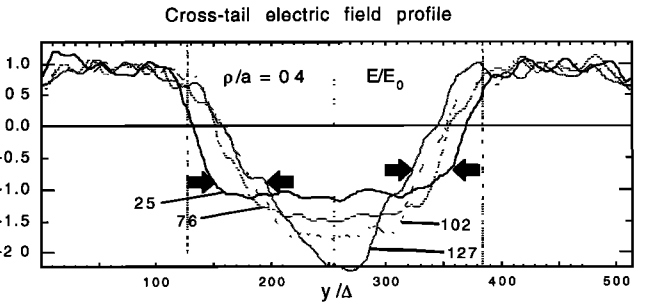

Figure 8. Time history of cross-tail electric field profiles ($\rho_i/a = 0.4$). E_y is normalized by the initial magnetosheath electric field E_0. As the K-H instability transports tailward momentum across the magnetopause, the velocity shear layer migrates towards the center of the simulation box. The electric potential Φ is conserved across each of the boundaries, but increased gradients in this quantity lead to a substantial enhancement of the dawn-dusk field across the center.

the lack of mixing on the dawnside that accounts for the shelf structure in the density profiles.

In Figure 8 profiles of E_y, normalized by the initial magnetosheath electric field E_0, are shown for different times. These indicate that as the magnetosphere is compressed, the negative (dawn-to-dusk) region is squeezed inward, but is accompanied by a strong increase in the strength of E. When integrating the electric field from the magnetosheath into the magnetosphere, we find that the potential Φ is conserved over time. In other words, as the magnetosphere width is reduced the dawn-to-dusk field increases inversely.

3.3. Heating Versus Mixing

The K-H instability produces a significant alteration of the particle distributions, by both mixing of the different plasma populations, and by heating via momentum transfer between the magnetosheath and magnetosphere particles. It is not possible to separate mixing effects from heating effects in observed distributions. In particle simulations, however, the particles are individually tracked, so the amount of mixing can be determined directly. Ion distributions in the dusk LLBL at $\Omega_i^{sp}t = 102$ are shown in Figure 9. Dawnside ion distributions are given in Figure 10. The left, middle, and right columns show two-dimensional distributions, and v_x- and v_y-reduced distributions, respectively. The sampling regions of the simulation box for each row are indicated by the insets in the left panels. In each one-dimensional frame there are three curves: (1) an exterior solid line, which is the final distribution at $\Omega_i^{sp}t = 102$, (2) an interior solid line, showing an early "quasi-equilibrium" distribution at $\Omega_i^{sp}t = 13$, and (3) a dotted line, showing a composite distribution for comparison. The composite distribution is constructed from initial magnetosphere and magnetosheath distributions, which are combined in the proportions found for the two ion populations at $\Omega_i^{sp}t = 102$. These represent the effect of simply mixing the original distributions. The shaded regions show the differences between the actual distributions at $\Omega_i^{sp}t = 13$ and $\Omega_i^{sp}t = 102$. The number at the top of each reduced v_y distribution indicates the percentage of magnetosphere ions present at $\Omega_i^{sp}t = 13$, and the number below it gives the percentage at $\Omega_i^{sp}t = 102$. All plots are logarithmic.

While the particle counts indicate penetration of magnetosheath plasma into the magnetosphere, and some increases in magnetosphere plasma in the magnetosheath, it is clear that the main changes in the distributions are due to heating. For example, the mid-LLBL frames in Figure 10 show temperatures which exceed the initial magnetosphere temperature, even though they can contain only a small fraction of magnetosphere population particles. The composite distributions, which present a simplified picture of what would occur with just mixing, are clearly cooler than the actual distributions at $\Omega_i^{sp}t = 102$.

The duskside distributions (Figure 9) show limited heating, with most of this occuring within the current layer (middle row). There is more heating transverse to the flow direction (i.e., in v_y). Despite considerable distortion of the shape of the magnetopause by this time, the gradient drift-induced high-energy tails seen in the $\Omega_i^{sp}t = 13$ distributions remain through $\Omega_i^{sp}t = 102$.

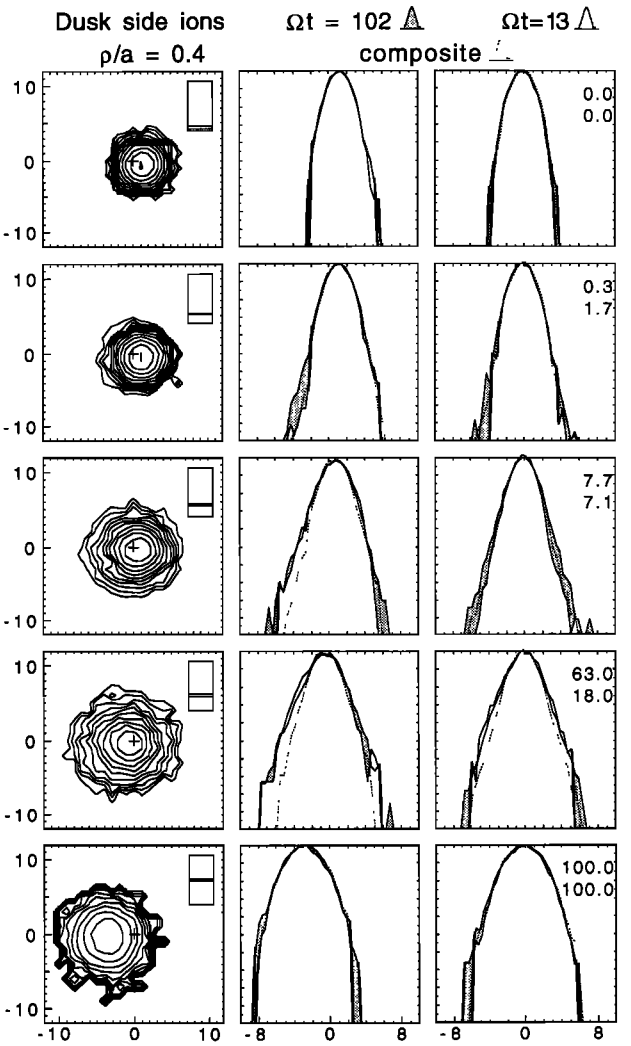

Figure 9. Dusk ion distributions ($\rho_i/a = 0.4$; $\Omega_i^{sp}t = 102$). On the left are two-dimensional distributions for ions located in the regions shown by the insets. Next to these are x and y distributions for the same samples. The one-dimensional frames include distributions at $\Omega_i^{sp}t = 13$ (inner solid curves), at $\Omega_i^{sp}t = 102$ (exterior solid curves), and composite distributions (dashed curves). The composite distributions represent a simple mixing distribution described in the text. The shaded areas show heating of the actual distributions between the early and late times. Velocities are given in units of v_{ti}^{sh}.

Within the LLBL on the dawnside (Figure 10) there is considerable heating in both v_x and v_y. In the current layer (middle row), somewhat stronger heating in v_x has tended to equalize the transverse and parallel temperatures. Within the transition regions (second and fourth rows), the heating instead is greatest in v_y, and this increases the asymmetry between v_x and v_y. The exterior transition region retains the high-energy tail in v_x caused by gradient drifts, but this is no longer

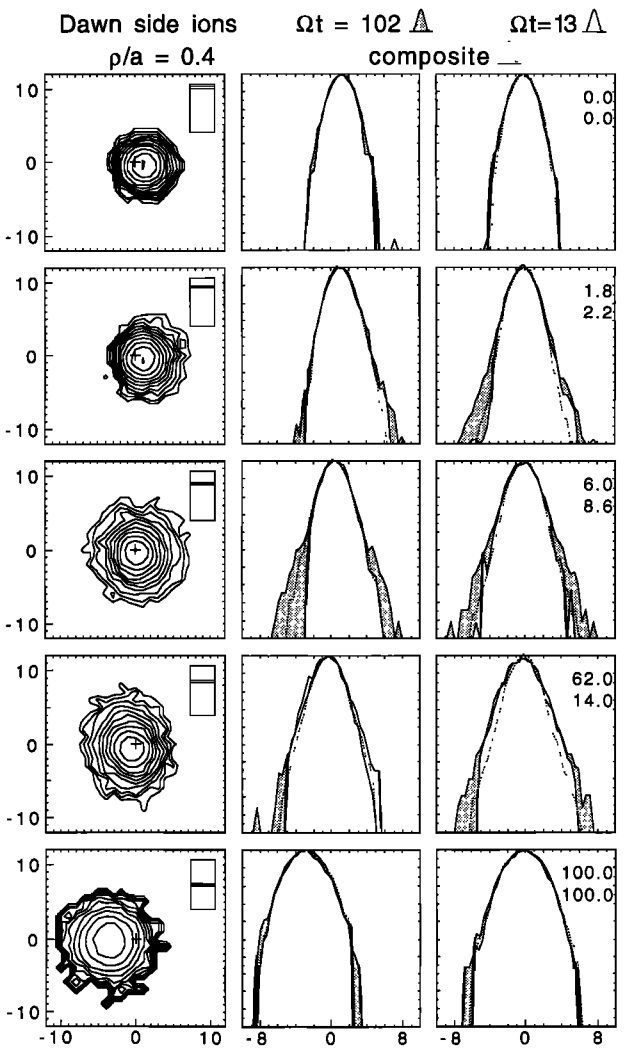

Figure 10. Dawn ion distributions ($\rho_i/a = 0.4$; $\Omega_i^{sp}t = 102$). These show greater heating within the magnetopause than is seen on the duskside.

apparent in the current layer and the interior transition region. Close inspection of Figures 9 and 10 shows that the exterior transition layer distribution (row 2) on the dawnside is hotter overall than the mirror distribution on the duskside, while the interior transition region distribution (row 4) on the dusk side is hotter than its dawn counterpart. This may be a reflection of the migration of hot particles along the **E** direction discussed above. Differences between the various boundary layer distributions should be observable. The forms for the distributions seen at $\Omega_i^{sp}t = 13$ should correspond to quiet LLBL crossings, while the final distributions should match active crossings.

3.4. Variation of the K-H Instability With Boundary Layer Thickness

In this section we compare results of the above case, where $\rho_i/a = 0.4$, with simulation runs having different initial boundary layer thicknesses ($\rho_i/a = 0.8$ and $\rho_i/a = 0.25$). All other parameters were left unchanged.

Figure 11 shows magnetosheath electron momentum vectors and number density contours at times approaching saturation for the narrow $\rho_i/a = 0.8$ case. For this thinner LLBL the asymmetries in the dawnside and duskside activation of the K-H instability is much more pronounced. Here the duskside disturbances began with a mode number of 4, which are apparent at $\Omega_i^{sp}t = 26$, and these vortices coalesce into a single mode by $\Omega_i^{sp}t = 102$. The dawnside, however, does not show significant growth prior to $\Omega_i^{sp}t = 51$, with the marginal perturbation shown at $\Omega_i^{sp}t = 127$ being the largest size attained by that disturbance. The duskside shows vortex motions characteristic of the behavior in the dusk LLBL for the first simulation, but the dawnside does not develop a coherent, strongly penetrating "tongue".

The development of the K-H instability on the duskside is also of interest because the ratio $\rho_i/a = 0.8$

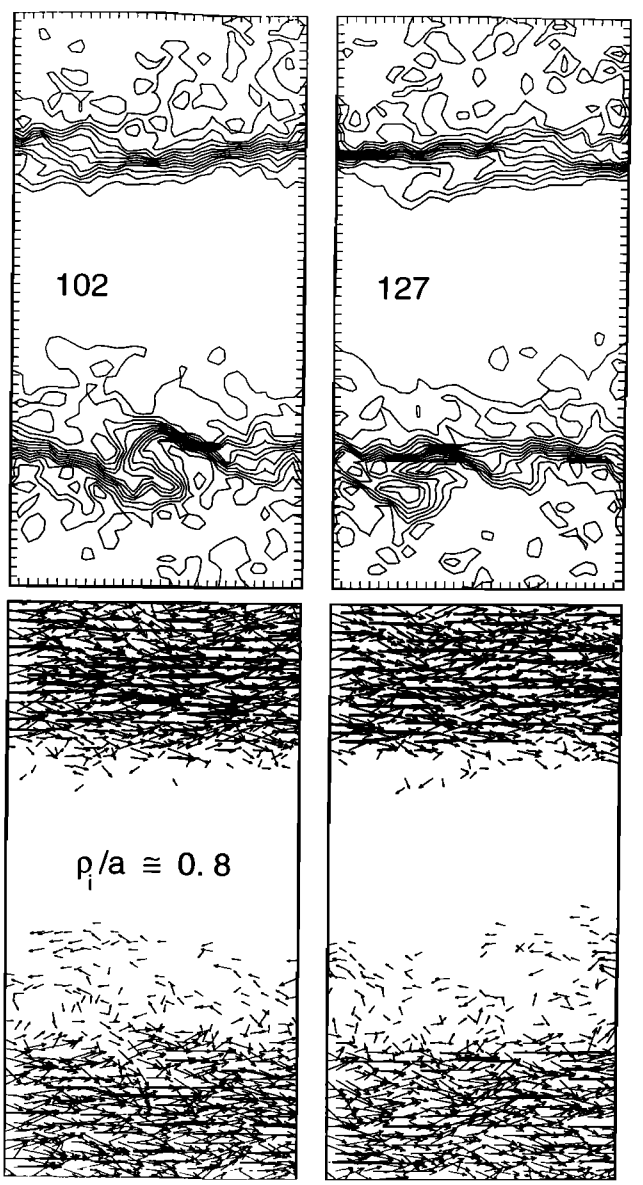

Figure 11. Magnetosheath electron momentum vectors and number densities for $\rho_i/a = 0.8$. Times correspond to near-saturation.

exceeds the suppression limit found by *Pritchett and Coroniti* [1984]. The difference is that in their simulation flat density, temperature and magnetic field profiles were assumed. When we ran a simulation using those conditions, we obtained results comparable to theirs, with similar growth rates. In the present case there are significant gradients in these physical quantities which, as discussed earlier, lead to an increased spread in the flow-parallel temperature $T_{i\parallel}$ of ions in the dusk boundary layer that enhances the development of the instability.

Results for a wider initial boundary layer ($\rho_i/a = 0.25$) are shown in Figure 12. The system evolved in a manner similar to that of the original case, with the formation of a penetrating tongue on the dawn side, and vortices on the duskside. One difference between the $\rho_i/a = 0.4$ and $\rho_i/a = 0.25$ runs is that in the latter case the onset of dawnside and duskside instabilities is apparent at nearly the same time $\sim \Omega_i^{sp} t = 51$.

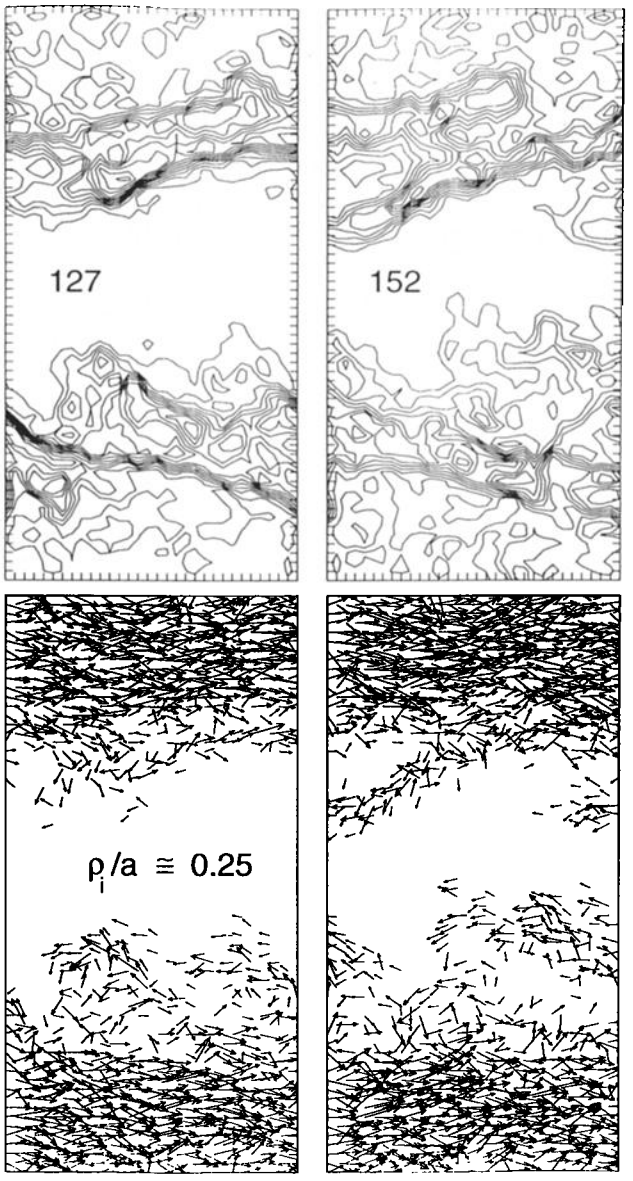

Figure 12. Magnetosheath electron momentum vectors and number densities at saturation for $\rho_i/a = 0.25$.

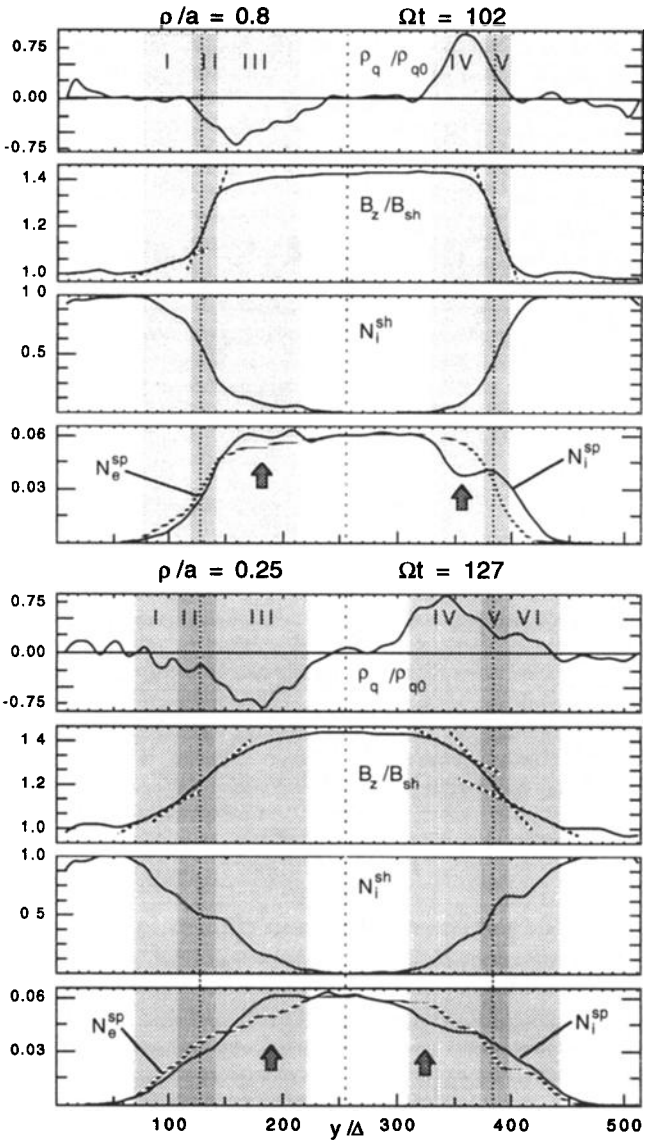

Figure 13. Profiles for (top) $\rho_i/a = 0.8$ and (bottom) $\rho_i/a = 0.25$. As before, ρ_q, B_z, and particle densities are averaged over x. Shaded regions highlight magnetopause structures that are formed in the LLBL on the two sides of the magnetosphere. (See text for explanation.)

The charge, magnetic field and density profiles for the thinner LLBL run, with $\rho_i/a = 0.8$ (Figure 13), reveal charge layers interior to the boundary layer surrounded by current layers, as was the case previously. In addition, there is the same shifting of magnetosphere ions along **E** (indicated by arrows) that was seen in the original case study. The dusk charge layer has been broadened considerably by the development of the K-H instability, while the dawn profile has broadened by only a small fraction of its original width. This broadening coincides with the greater magnetosheath penetration on the duskside. Both the dawn and dusk current layers (dark shading in the B_z profile) are sharp, but the dusk-

side has an exterior wing much like the sheath transition layer identified by *Song et al.* [1990]. As the magnetic field there increases, the magnetosheath particle density decreases in a corresponding linear fashion. The local maximum of N_i^{sp}, resulting from the hot magnetosphere ion drifts along **E**, is located within the dusk current layer. This is consistent with the finite Larmor radius effects that cause the charge migration being strongest where the magnetic field gradients are largest. The duskside LLBL, for which the interior and exterior transition layers are identifiable, has a final width of approximately 1400 km at $\Omega_i^{sp}t = 102$.

The $\rho_i/a = 0.25$ profiles show charge layers which have migrated in toward the magnetosphere, but these are rather symmetric across the dawnside and duskside. On the dusk side the magnetic field has the three constant-slope regions seen for the $\rho_i/a = 0.4$ case, corresponding to an exterior transition layer, a current layer, and an interior transition layer. The match to the overall properties described by *Song et al.* [1990] for the corresponding layers is not as strong for this case as for the $\rho_i/a = 0.4$ run. When the transition layers are included, the widths of the dusk and dawn LLBLs at $\Omega_i^{sp}t = 127$ are about 1600 and 1300 km, respectively. These widths represent final boundary layer thicknesses that are only fractionally larger than seen in the $\rho_i/a = 0.8$ case, which began with a current layer 1/3 the size.

Cross-tail electric field profiles for the narrow and wide boundary layer runs are shown in Figure 14. In both cases these indicate increases of the dawn-to-dusk field with time as the velocity shear layer encroaches upon the magnetosphere. In addition the peak of the field shifts toward the dawnside, reflecting the deeper plasma penetration on the dusk side. Also evident in the figures is the increase of this asymmetry with decreasing a. The $\rho_i/a = 0.4$ run shows the greatest maximum dawn-to-dusk field strength, but this may result from the $\rho_i/a = 0.25$ saturation being artificially constrained by the system size. In all cases the electric field increases so that the potential across the magnetosphere is conserved.

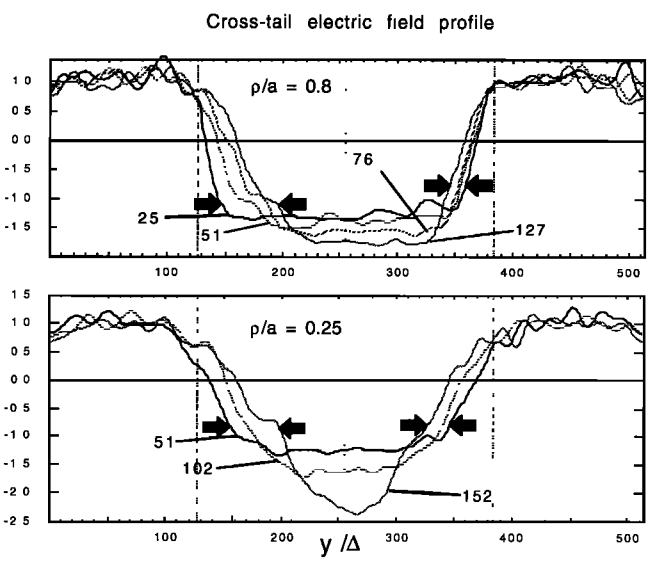

Figure 14. Time history of E_y for $\rho_i/a = 0.8$ and $\rho_i/a = 0.25$. These show profiles of the cross-tail electric field at times given. Arrows indicate velocity shear layers, which are more asymmetric for the $\rho_i/a = 0.8$ case.

4. Summary and Discussion

Two-dimensional, electromagnetic particle simulations have been used to study the K-H instability in a simplified geometry that incorporates both the dawnside and the duskside of the LLBL. We have shown the likely existence of dawn-dusk asymmetries developing in the LLBL due to the evolution of the instability. These asymmetries arise from kinetic effects that are not included in fluid MHD studies. In particular, equilibrium distributions show an enhanced spread in v_x for ions on the duskside, and an enhanced spread in v_y on the dawnside, which are due to particle motions associated with convective $\mathbf{E} \times \mathbf{B}$ drifts in the presence of electric field gradients, and from gradient drifts. The increased flow parallel temperature for ions $T_{i\parallel}$ on the duskside led to earlier onset of the K-H instability there, with small scale modes that later coalesced into larger modes. Dawnside disturbances emerged at later times, with larger initial wavelengths. Slow, **E**-aligned acceleration of ions in the presence of field gradients led to unequal penetration of ions and electrons into the magnetosphere on the dawn side, as was demonstrated in (Figure 6). The structures that emerge on the dawnside are more coherent than those on the duskside, and form thin filaments, characteristic of the hybrid studies of *Thomas and Winske* [1993].

Profiles of B_z and total charge highlight the emergence of distinct current and charge/transition layers in the dawn and dusk LLBLs. The centers of the current layers shift only slightly as a result of instability, while the charge layers are seen to shift in towards the magnetosphere and to broaden to $> 0.1R_E$, which compares with observed thicknesses. As downstream stresses are transported across the magnetopause, material interior to it acquires a downstream flow. A corresponding convective electric field accompanies the flow, and this requires the migration of the charge layer. In the dawn side LLBL we see boundary layer structures emerge which are similar to those found in dayside magnetopause crossings identified by *Song et al.* [1990]. These include regions with characteristics of the sheath transition layer, a sharp current layer, and the outer boundary layer. As the charge layers migrate in toward the magnetosphere, the region of dusk-to-dawn pointing **E** (tailward flow) widens, while the dawn-to-dusk region narrows. As the dawn-to-dusk region is compressed, there is a corresponding increase in field strength there. This increase is consistent with the amount needed to maintain a constant electric potential Φ in the interior.

Our particle simulations allow for direct measurement of particle mixing and of particle heating through the construction of distribution functions. Observed

changes in the distributions are mainly due to heating within the boundary layers, where counterstreaming flows are interacting, and are particularly strong in the dawnside LLBL. At the center of the dawn boundary layer (i.e., in the current layer) the primarily magnetosheath particles are heated to temperatures in excess of the magnetosphere temperature, with a greater heating in v_x leading to equal temperatures in both directions. Within the interior and exterior transition regions on this side, greater heating in the transverse direction led to additional asymmetry in v_x and v_y. Such changes in the dawnside distributions should be observable by comparing measurements during active and inactive satellite crossings.

Simulations with different initial boundary layer thicknesses a show that as ρ_i/a is increased the asymmetries between dawnside and duskside behavior increase. For $\rho_i/a = 0.8$ the duskside develops fluidlike vortexes, but the dawnside perturbation fails to grow very large, and never pushes past the dawnside charge layer. This thin boundary layer case shows asymmetry in the profiles of total charge, which can be attributed to the significant reduction of magnetosheath plasma penetration on the dawnside. All trials show an increase in the dawn-to-dusk electric field as the magnetosphere is compressed, but the $\rho_i/a = 0.8$ case shows a greater displacement of the peak E value towards the dawn side, corresponding to the asymmetric penetration of magnetosheath plasma in that trial. Velocity distributions for the narrow and wide runs evolve in the same manner as do those for the $\rho_i/a = 0.4$ case.

If ρ_i/a were decreased to values much smaller than 0.25, we expect that the dawn-dusk asymmetries reported here would diminish, ultimately recovering the symmetric case that results from a MHD treatment. In section 3 we argued that the observed differences in the activation of the K-H instability resulted from anisotropies in the early velocity distributions. However, in the thick boundary limit, particles would sample nearly uniform fields over their gyro-orbits, and their equilibrium distributions would be isotropic. In an analytic treatment of velocity shears perpendicular to $\mathbf{B}$, *Ganguli et al.* [1988a] obtained an explicit form for the distributions which bear out this ρ_i/a dependence on the isotropy at equilibrium.

The results we have presented must be viewed in the context of our model's limitations. Problematic aspects of our approach include the simplistic two-dimensional geometry employed, the restrictions on physical scales, and the means for establishing equilibrium. Our choice of $\mathbf{k} \cdot \mathbf{B} = 0$ does not allow for excitation of electrostatic ion cyclotron modes which may significantly contribute to the structure and dynamics of the magnetosphere [*Ganguli et al.*, 1988a, 1991], particularly when field-aligned potentials are strong. Recently, *Miura and Kan* [1992] and *Wei and Lee* [1993] have conducted fluid MHD studies of the K-H instability which model the effects of magnetosphere-ionosphere coupling via field-aligned currents. Finite conductivity in the ionosphere is seen to inhibit the growth of vortex structures, and this must be included in a future particle study.

The slab geometry used has been employed in all the earlier models cited in section 1, and here has allowed for ready inclusion of two interaction regions in one simulation box. Of course, a more realistic geometry for the LLBL should be curved, with the cross-tail electric field bowed in the interior. Nonetheless, we believe that most of the qualitative features of our model would persist in a such a geometry. The formation of distinct charge and current layers, for example, occurs in spite of the large amount of curvature introduced by the perturbations themselves. Work is in progress to develop a driven two-dimensional system, which will not be subject to initial value equilibrium requirements, and this will be employed to study the K-H instability under varying solar wind conditions.

Acknowledgments. This work was supported by National Science Foundation grant ATM 92-96075, and NASA Graduate Student Researchers Program Fellowship 93-353. Some computing resources were provided by the San Diego Supercomputing Center, which is supported by the NSF.

The Editor thanks C-Q. Wei and G. Ganguli for their assistance in evaluating this paper.

References

Allan, W., and E.M. Poulter, The spatial structure of different ULF pulsation types: A review of stare radar results, *Rev. Geophys., 22,* 85, 1984.

Atkinson, G., and T. Watanabe, Surface waves on the magnetosphere boundary as a possible origin of long period micropulsations, *Earth Planet. Sci. Lett., 1,* 89, 1966.

Axford, W.I., and C.O. Hines, A unifying theory of high-latitude geophysical phenomena and geomagnetic storms, *Can. J. Phys., 39,* 1433, 1961.

Belmont, G., and G. Chanteur, Advances in magnetopause Kelvin-Helmholtz instability studies, *Phys. Scr., 40,* 124, 1989.

Berchem, J., and C.T. Russell, The thickness of the magnetopause current layer: ISEE 1 and 2 observations, *J. Geophys. Res., 87,* 2108, 1982.

Blumen, W., P.G. Drazin and D.F. Billings, Shear layer instability of an inviscid compressible fluid, 2, *J. Fluid Mech., 71,* 305, 1975.

Cai, D., R.O. Storey, and T. Neubert, Kinetic equilibria of plasma shear layers, *Phys. Fluids B, 2* 75, 1990.

Chandrasekhar, S., *Hydrodynamic and Hydromagnetic Stability,* Clarendon, Oxford, 1961.

Couzens, D.A., G.K. Parks, K.A. Anderson, R.P. Lin, and H. Reme, ISEE particle observations of surface waves at the magnetopause boundary layer *J. Geophys. Res., 90,* 6343, 1985.

Drazin, P.G., and A. Davey, Shear layer instability of an inviscid compressible fluid, *J. Fluid Mech., 82,* 255, 1977.

Dungey, J.W., Electrodynamics of the outer atmosphere, in *Proceedings of the Ionosphere Conference,* p. 225, The Physical Society of London, London, 1955.

Dungey, J.W., *Cosmic Electrodynamics,* p. 183, Cambridge University Press, New York, 1958.

Dungey, J.W., Interplanetary magnetic field and the auroral zones, *Phys. Rev. Lett, 6,* 47, 1961.

Dungey, J.W., The theory of the quiet magnetosphere, in *Solar Terrestrial Physics,* p.91 , Academic Press, London, 1967.

Dungey, J.W., and D.J. Southwood, Theory of ULF waves in the magnetosphere, *Space Sci. Rev., 10,* 672, 1970.

Fejer, J.A., Hydromagnetic stability at a fluid velocity discontinuity between compressible fluids, *Phys. Fluids, 7,* 499, 1964.

Fujimoto, M., and T. Teresawa, Ion inertia effect on the Kelvin-Helmholtz instability, *J. Geophys. Res., 96,* 15,725, 1991.

Ganguli, G., Y.C. Lee, and P. Palmadesso, Electrostatic ion-cyclotron instability caused by a nonuniform electric field perpendicular to the external magnetic field, *Phys. Fluids, 28,* 761, 1985.

Ganguli, G., Y.C. Lee, and P. Palmadesso, Kinetic theory for electrostatic waves due to transverse velocity shears, *Phys. Fluids, 31,* 823, 1988a.

Ganguli, G., Y.C. Lee, and P. Palmadesso, Electron-ion hybrid mode due to transverse velocity shear *Phys. Fluids, 31,* 2753, 1988b.

Ganguli, G., Y.C. Lee, P.J. Palmadesso, and S.L. Ossakow, Oscillations in a plasma with parallel currents and transverse velocity shears, *Phys. Space Plasmas, 8,* 231, 1988c.

Ganguli, G., Y.C. Lee, and P.J. Palmadesso, Role of small scale processes in global plasma modeling, in Modeling Magnetospheric Plasma Processes, *Geophys. Monogr. Ser.,* vol. 62, edited by G.R. Wilson, p. 17, AGU, Washington, D.C., 1991.

Haerendel, G., G. Paschmann, N. Sckopke, H. Rosenbauer, and P.C. Hedgecock, The frontside boundary layer of the magnetosphere and the problem of reconnection, *J. Geophys. Res., 83,* 3195, 1978.

Lui, A.T.Y., D. Venkatesan, and J.S. Murphree, Auroral bright spots on the dayside oval, *J. Geophys. Res., 94,* 5515, 1989.

Mitchell, D.G., F. Kutchko, D.J. Williams, T.E. Eastman, L.A. Frank, and C.T. Russell, An extended study of the low-latitude boundary layer on the dawn and dusk flanks of the magnetosphere, *J. Geophys. Res., 92,* 7394, 1987.

Miura, A., Nonlinear evolution of the magnetohydrodynamic Kelvin-Helmholtz instability, *Phys. Rev. Lett, 49,* 779, 1982.

Miura, A., Anomalous transport by magnetohydrodynamic Kelvin-Helmholtz instabilities in the solar wind-magnetosphere interaction, *J. Geophys. Res., 89,* 801, 1984.

Miura, A., Simulation of Kelvin-Helmholtz instability at the magnetospheric boundary, *J. Geophys. Res., 92,* 3195, 1987.

Miura, A., Kelvin-Helmholtz instability for supersonic shear flow at the magnetospheric boundary, *Geophys. Res. Lett., 17,* 749, 1990.

Miura, A., Kelvin-Helmholtz instability at the magnetospheric boundary: Dependence on the magnetosheath sonic mach number, *J. Geophys. Res., 97,* 10,655, 1992.

Miura, A., and Kan, J.R., Line-tying effects on the Kelvin-Helmholtz instability, *Geophys. Res. Lett., 19,* 1611, 1992.

Miura, A., and P.L. Pritchett, Nonlocal stability ananlysis of the MHD Kelvin-Helmholtz instability in a compressible plasma, *J. Geophys. Res., 87,* 7431, 1982.

Nishikawa, K.-I., G. Ganguli, Y.C. Lee, and P.J. Palmadesso, Simulation of ion-cyclotron-like modes in a magnetoplasma with transverse inhomogeneous electric field, *Phys. Fluids, 31,* 1568, 1988.

Nishikawa, K.-I., G. Ganguli, Y.C. Lee, and P.J. Palmadesso, Simulation of electrostatic turbulence due to sheared flows parallel and transverse to the magnetic field, *J. Geophys. Res., 95,* 1029, 1990.

Opp, E.N., and A.B. Hassam, Kelvin-Helmholtz instability in systems with large effective Larmor radius, *Phys. Fluids, 3,* 885, 1991.

Papamoschou, D., and A. Roshko, The compressible turbulent shear layer: An experimental study, *J. Fluid Mech., 197,* 453, 1988.

Petscheck, H.E., Magnetic field annihilation, *NASA Spec. Publ., SP-50,* 425, 1964.

Pritchett, P.L., Electrostatic Kelvin-Helmholtz instability produced by a localized electric field perpendicular to an external magnetic field, *Phys. Fluids, 30,* 272, 1987.

Pritchett, P.L., and F.V. Coroniti, The collisionless macroscopic Kelvin-Helmholtz instability 1: Transverse electrostatic mode, *J. Geophys. Res., 89,* 168, 1984.

Pu, Z., and M.G. Kivelson, Kelvin-Helmholtz instability at the magnetopause: solution for compressible plasmas, *J. Geophys. Res., 88,* 841, 1983.

Romero, H., G. Ganguli, and Y.C. Lee, Ion acceleration and coherent structures generated by lower hybrid shear-driven instabilities, *Phys. Rev. Lett, 69,* 3503, 1992.

Romero, H., and G. Ganguli, Relaxation of the stressed plasma sheet boundary layer, *Geophys. Res. Lett., 21,* 6455, 1994.

Sckopke, N., G. Paschmann, B.U.Ö. Sonnerup, S.J. Bame, T.G. Forbes, E.W. Hones Jr., and C.T. Russell, Structure of the low-latitude boundary layer, *J. Geophys. Res., 86,* 2099, 1981.

Sen, A.K., The stability of the magnetospheric boundary, *Planet. Space Sci., 13,* 131, 1964.

Song, P., R.C. Elphic, C.T. Russell, J.T. Gosling, and C.A. Cattell, Structure and properties of the subsolar magnetopause for northward IMF: ISEE observations, *J. Geophys. Res., 95,* 6375, 1990.

Song, P., C.T. Russell, R.J. Fitzenreiter, J.T. Gosling, M.F. Thomsen, D.G. Mitchell, S.A. Fuselier, G.K. Parks, R.R. Anderson, and D. Hubert, Structure and properties of the subsolar magnetopause for northward interplanetary magnetic field: Multiple-instrument particle observations, *J. Geophys. Res., 98,* 11,319, 1993.

Southwood, D.J., The hydromagnetic stability of the magnetospheric boundary, *Planet. Space Sci., 16,* 587, 1968.

Teresawa, T., M. Fujimoto, H. Karimabadi, and N. Omidi, Anomalous ion mixing within a Kelvin-Helmholtz vortex in a collisionless plasma, *Phys. Rev. Lett, 68,* 2778, 1992.

Thomas, V.A., and D. Winske, Kinetic simulation of the Kelvin-Helmholtz instability at the magnetopause, *Geophys. Res. Lett., 18,* 1943, 1991.

Thomas, V.A., and D. Winske, Kinetic simulation of the Kelvin-Helmholtz instability at the magnetopause, *J. Geophys. Res., 98,* 11,411, 1993.

Wang, Z., P.L. Pritchett, and M. Ashour-Abdalla, Kinetic effects on the velocity-shear-driven instability, *Phys. Fluids, 4,* 1092, 1992.

Wei, C.Q., and L.C. Lee, Coupling of magnetopause-boundary layer to the polar ionosphere, *J. Geophys. Res., 98,* 5707, 1993.

Wei, C.Q., L.C. Lee, and A.L. La Belle-Hamer, A simulation study of the vortex structure in the low-latitude boundary layer, *J. Geophys. Res., 95,* 20,793, 1990.

Williams, D.J., Magnetopause characteristics at 0840-1040 hours local time, *J. Geophys. Res., 85,* 3387, 1980.

Winglee, R.M., and P.J. Kellogg, Electron beam injection during active experiments, 1, Electromagnetic wave emissions, *J. Geophys. Res., 95,* 6167, 1990.

Wu, C.C., Kelvin-Helmholtz instability at the magnetopause boundary, *J. Geophys. Res., 91,* 3042, 1986.

M. Wilber and R. M. Winglee, Geophysics Program AK-50, University of Washington, Seattle, WA 98195. (e-mail: wilber@geophys.washington.edu)

(Received February 7, 1994; revised September 8, 1994; accepted September 14, 1994.)